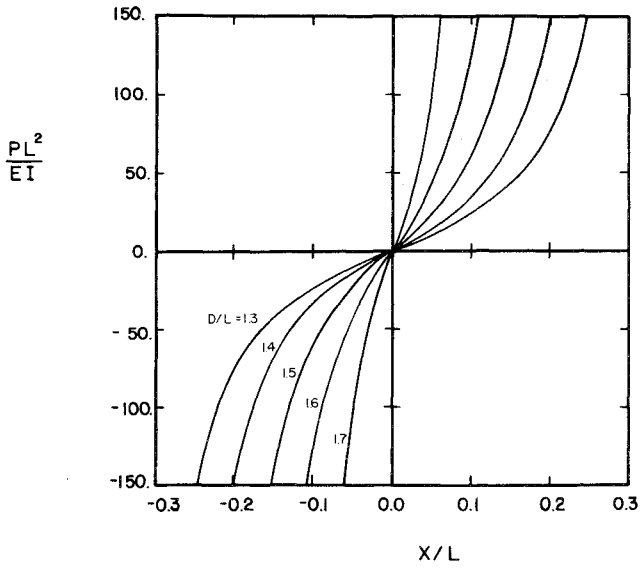

Fig. 2 Nondimensional load-deflection behavior for the adjustable "elastica" spring.

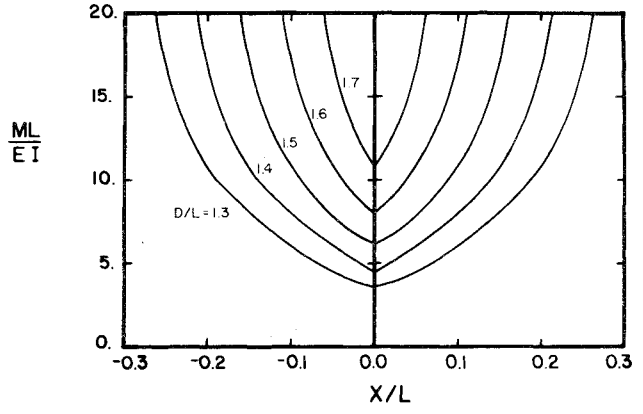

Fig. 3 Nondimensional maximum bending moment-deflection behavior for the adjustable "elastica" spring.

Using these two mathematical forms, the requirement that $W_u + W_n = D$ and the requirement that the overall load P must be the combination of the loads P_u and P_n, the designer can find the load and maximum bending moment for any deflection of the device shown in Fig. 1. The nondimensional load-vs-deflection curve is shown in Fig. 2 for various values of D. The bending stress will be maximum wherever the bending moment is maximum. This critical value will occur at the point where the curvature of the strip is maximum. For the design process, the value of M can be determined from the nondimensional plot shown in Fig. 3. Since the strips are assumed to be initially straight before they are installed, the bending moment does not equal zero when the suspension deflection is zero.

Once the parameter D has been selected, the dynamic analysis can be accomplished by traditional techniques.[4] When properly applied, the elastica suspension allows an initial "soft" support to minimize steady-state vibration transmission but will also stiffen at large deflections to provide "hard" behavior in the presence of shock loads. The selection of the parameter D allows the designer to choose the degree of initial stiffness necessary for a particular application.

Acknowledgment

The first author gratefully acknowledges the financial assistance of the University of Houston, Engineering Systems Simulation Lab, for their support of this investigation.

References

[1] Efstathiades, G. J. and Williams, C. J. H., "Vibration Isolation Using Non-Linear Springs," *International Journal of Mechanical Science*, Vol. 9, No. 1, 1967, pp. 27-44.

[2] Shoup, T. E., "Experimental Investigation of a Nonlinear Elastic Suspension," *AIAA Journal*, Vol. 10, April 1972, pp. 559-560.

[3] Frish-Fay, R., *Flexible Bars*, Butterworth & Co. Ltd., London, England, 1962.

[4] Stoker, J. J., *Nonlinear Vibrations*, Interscience, New York, 1950.

Motion of Spinning Spacecraft with Hinged Appendages

R. Sellappan* and P.M. Bainum†
Howard University, Washington, D.C.

Introduction

THE motion and stability of a spin-stabilized spacecraft with hinged appendages are treated. The dynamics of this type of fixed length appendage system during the deployment maneuver has been previously studied only for the case where the transverse components of the angular velocity vector are assumed to be zero throughout deployment and where the hinge points are located on the hub's principal transverse axes.[1] The present study considers the three-dimensional dynamics of a spin-stabilized spacecraft with hinged appendages where there is no restriction on the location of the hinge points. The motion and stability of such a system will be studied, analytically for special cases, and numerically for the general case.

Analysis

A. Equations of Motion

The hinged system to be studied is shown schematically in Fig. 1. The equations of motion in the five variables: ω_1, ω_2, ω_3, α_1, and α_2 are developed using the quasi-Lagrangian formulation for ω_i, $i=1,2,3$, and the general Lagrangian formulation for the variables α_i, $i=1,2$. The equations of motion for this system, neglecting external torques, are obtained as follows $[m/(M+2m) << 1]$[2]:

$$I_1\dot{\omega}_1 - (I_2 - I_3)\omega_2\omega_3 + m[2(r_0^2 + a^2 + \ell^2) + 2\ell\{r_0(s\alpha_1 + s\alpha_2) - a(c\alpha_1 + c\alpha_2)\}]\dot{\omega}_1 - m\{2a^2 - 2a\ell(c\alpha_1 + c\alpha_2) + \ell^2(c2\alpha_1 + c2\alpha_2) - 2r_0^2 - 2r_0\ell(s\alpha_1 + s\alpha_2)\}\omega_2\omega_3 + 2m\ell\{r_0(c\alpha_1\dot{\alpha}_1 + c\alpha_2\dot{\alpha}_2) + a(s\alpha_1\dot{\alpha}_1 + s\alpha_2\dot{\alpha}_2)\}\omega_1 + m\ell\{a \times (s\alpha_1 - s\alpha_2) - r_0(c\alpha_1 - c\alpha_2) - (\ell/2)(s2\alpha_1 - s2\alpha_2)\} + (\omega_3^2 - \omega_2^2) + m\{\ell\{\ddot{\alpha}_1 - \ddot{\alpha}_2) + (\dot{\alpha}_1)^2(r_0c\alpha_1 + as\alpha_1) + \ddot{\alpha}_1(r_0s\alpha_1 - ac\alpha_1) - (\dot{\alpha}_2)^2(r_0c\alpha_2 + as\alpha_2) - \ddot{\alpha}_2(r_0s\alpha_2 - ac\alpha_2)\} = 0 \quad (1)$$

$$I_2\dot{\omega}_2 - (I_3 - I_1)\omega_3\omega_1 + m\{2a^2 - 2a\ell(c\alpha_1 + c\alpha_2) + \ell^2(c^2\alpha_1 + c^2\alpha_2)\}\dot{\omega}_2 - m\ell\{a(s\alpha_1 - s\alpha_2) - r_0(c\alpha_1 - c\alpha_2) - (\ell/2)(s2\alpha_1 - s2\alpha_2)\}\dot{\omega}_3 + m\ell\{a(s\alpha_1 - s\alpha_2) - r_0(c\alpha_1 - c\alpha_2) - (\ell/2)(s2\alpha_1 - s2\alpha_2)\}\omega_1\omega_2$$

Presented as Paper 76-784, at the AIAA/AAS Astrodynamics Conference, San Diego, Calif., Aug. 18-20, 1976; submitted Sept. 13, 1976; revision received Feb. 28, 1977.

Index category: Spacecraft Attitude Dynamics and Control.

*Senior Graduate Research Assistant, Dept. of Mechanical Engineering. Student Member AIAA.

†Professor of Aerospace Engineering, Dept. of Mechanical Engineering. Associate Fellow AIAA.

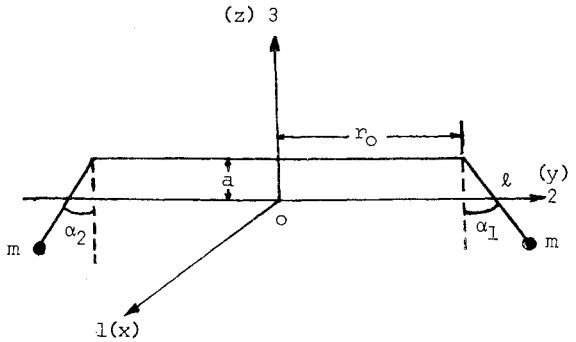

Fig. 1 Hinged deployment system.

$$-m\{\ell^2(s^2\alpha_1+s^2\alpha_2)-2(a^2+\ell^2)+2\ell a(c\alpha_1+c\alpha_2)\}\omega_3\omega_1+m\{2a\ell(s\alpha_1\dot{\alpha}_1+s\alpha_2\dot{\alpha}_2)-\ell^2(s2\alpha_1\dot{\alpha}_1+s2\alpha_2\dot{\alpha}_2)\}\omega_2+m\ell\{\ell(\dot{\alpha}_1-\dot{\alpha}_2)-2a(c\alpha_1\dot{\alpha}_1-c\alpha_2\dot{\alpha}_2)+\ell(c2\alpha_1\dot{\alpha}_1-c2\alpha_2\dot{\alpha}_2)\}\omega_3=0 \tag{2}$$

$$I_3\dot{\omega}_3-(I_1-I_2)\omega_1\omega_2+m\{2r_0^2+2r_0\ell(s\alpha_1+s\alpha_2)+\ell^2(s^2\alpha_1+s^2\alpha_2)\}\dot{\omega}_3-m\ell\{a(s\alpha_1-s\alpha_2)-r_0(c\alpha_1-c\alpha_2)-(\ell/2)(s2\alpha_1-s2\alpha_2)\}\dot{\omega}_2-m\{2(r_0^2+\ell^2)+2\ell r_0(s\alpha_1+s\alpha_2)-\ell^2(c^2\alpha_1+c^2\alpha_2)\}\omega_1\omega_2-m\ell\{a(s\alpha_1-s\alpha_2)-r_0(c\alpha_1-c\alpha_2)-(\ell/2)(s2\alpha_1-s2\alpha_2)\}\omega_3\omega_1-m\ell\{2r_0(s\alpha_1\dot{\alpha}_1-s\alpha_2\dot{\alpha}_2)-\ell(c2\alpha_1\dot{\alpha}_1-c2\alpha_2\dot{\alpha}_2)+\ell(\dot{\alpha}_1-\dot{\alpha}_2)\}\omega_2+m\{2r_0\ell(c\alpha_1\dot{\alpha}_1+c\alpha_2\dot{\alpha}_2)+\ell^2(s2\alpha_1\dot{\alpha}_1+s2\alpha_2\dot{\alpha}_2)\}\omega_3=0 \tag{3}$$

$$\ell\ddot{\alpha}_i\pm(\ell+r_0s\alpha_i-ac\alpha_i)\dot{\omega}_1-(r_0c\alpha_i+(\ell/2)s2\alpha_i)\omega_3^2-(as\alpha_i-(\ell/2)s2\alpha_i)\omega_2^2-(r_0c\alpha_i+as\alpha_i)\omega_1^2\pm(ac\alpha_i+r_0s\alpha_i-\ell c2\alpha_i)\omega_3\omega_2+(c_\alpha/m)\ell\dot{\alpha}_i=0 \tag{4}$$

Here, we define $s\alpha_i\equiv\sin\alpha_i$ and $c\alpha_i\equiv\cos\alpha_i$. Also, where a sign option exists, the upper sign applies for $i=1$ and the lower sign applies for $i=2$. (A linear viscous damping is assumed to be present about the hinge points with c_α the equivalent viscous damping coefficient.)

B. Two-Dimensional Motion

The equations of motion for the two-dimensional case with no offset can be obtained by assuming $\omega_1=\omega_2=a=0$. Also, following Ref. 1, the hinge members are assumed to move in-phase ($\alpha_1=\alpha_2=\alpha$). The equations are linearized about the nominal equilibrium state: $\alpha=\pi/2$ and $\omega_3=\Omega$ (Ω = nominal spin). The original coordinates can then be related to the variational coordinates by:

$$\alpha=\pi/2+\epsilon;\quad \omega_3=\Omega+\delta;\quad \epsilon<<1,\quad \delta<<\Omega \tag{5}$$

The linearized equations which result are:

$$\omega_3=\Omega+\delta(0)\simeq\Omega=\text{constant} \tag{6}$$

$$\ddot{\epsilon}+d_\alpha\dot{\epsilon}+\lambda^2\epsilon=0 \tag{7}$$

where

$$d_\alpha=c_\alpha/m\quad\text{and}\quad\lambda=\Omega\sqrt{1+r_0/\ell}$$

The stability of this second-order system is well known.

Next, the large amplitude case is considered. From Eq. (3), the closed-form solution relating the spin rate to the hinge angle, with the initial conditions: $\omega_3(0)=\Omega$, $\alpha(0)=0$, is

$$\omega_3(t)=\Omega(I_3+2m\,r_0^2)/[I_3+2m(r_0+\ell\sin\alpha)^2] \tag{8}$$

Here it is observed that $\omega_3(t)$ attains a maximum value when $\alpha=0,\pi$, etc., and a minimum when $\alpha=\pi/2, 3\pi/2$, etc.

C. Three-Dimensional Motion

The three-dimensional equations of motion, Eqs. (1-4), are linearized about the nominal equilibrium state: $\omega_1=\omega_2=0$, $\alpha_1=\alpha_2=\pi/2$, $\omega_3=\Omega$. The original coordinates are related to the variational coordinates by:

$$\alpha_i=\pi/2+\epsilon_i,\quad i=1,2;\quad \omega_3=\Omega+\delta \tag{9}$$

Based on the assumptions that ω_1/Ω, ω_2/Ω, δ/Ω, ϵ_i, and $\dot{\epsilon}_i/\Omega$ are small compared to 1, the equations of motion for a symmetrical spacecraft ($I_1=I_2=I$) can be approximated by a linear set in which $\omega_3=\Omega+\delta(0)\simeq\Omega$ is a constant. With $\tau=\Omega t$ as the independent variable, $u=\omega_1/\Omega$ and $v=\omega_2/\Omega$ as dependent variables, and

$$h=2ma^2/I,\quad g=2m(r_0+\ell)^2/I,\quad k=m\ell(r_0+\ell)/I$$

$$2\rho=c_\alpha/m\Omega,\quad f=1+(r_0/\ell),\quad n=(I_3/I)-1$$

as nondimensional constants, the linear equations become:

$$(1+g+h)u'+(n+g-h)v+k(\epsilon_1''+\epsilon_1)-k(\epsilon_2''+\epsilon_2)=0 \tag{10}$$

$$(1+h)v'-(n-h)u=0 \tag{11}$$

$$\epsilon_i''+2\rho\epsilon_i'+f\epsilon_i\pm fu'\pm fv=0;\quad i=1,2 \tag{12}$$

where primes denote derivatives with respect to τ, and the relationship: $g=2kf$ is used.

The necessary and sufficient conditions for stability of the system are obtained by applying the Routh-Hurwitz criterion similar to the procedure of Ref. 3. The characteristic equation, corresponding to Eqs. (10-12), is developed as

$$(s^2+2\rho s+f)[\{(1+g+h)(1+h)s^2+(n+g-h)(n-h)\}\times(s^2+2\rho s+f)-g(s^2+1)\{(1+h)s^2+(n-h)\}]=0 \tag{13}$$

Equation (13) separates into two factors – a second-order factor describing a mode where both hinged members move in phase as a unit, and a factor represented by a more complex fourth-order polynomial. From the quadratic factor the stability condition is found to be $c_\alpha>0$.

As the stability, also, depends on the fourth-order factor in Eq. (13), we will consider different configurations of the system in the following special cases:

Case a: I_3 maximum moment of inertia ($n>0$) with no offset of hinge points ($h=0$): the fourth-order factor in Eq. (13) with $h=0$ reduces to:

$$p_0s^4+p_1s^3+p_2s^2+p_3s+p_4=0 \tag{14}$$

where

$$p_0=1;\ p_1=2\rho(1+g);\ p_2=(n+g)n+(1+g)f-g(1+n);\ p_3=2\rho(n+g)n;\ p_4=(n+g)nf-gn$$

The nontrivial Routh-Hurwitz stability conditions are

$$p_1p_2-p_0p_3>0 \tag{15}$$

$$(p_1p_2-p_0p_3)p_3-p_1^2p_4>0 \tag{16}$$

Expansion of Inequalities (15) and (16) results in complex algebraic relationships involving the system parameters.

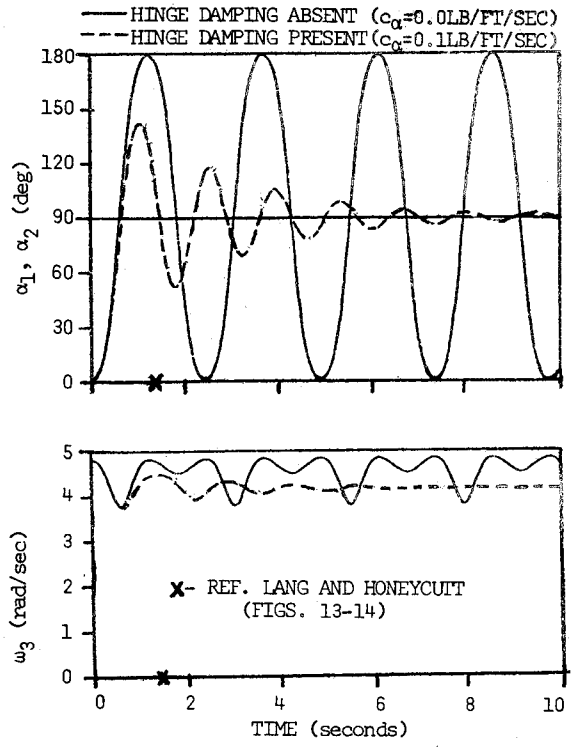

Fig. 2 Deployment dynamics of the system for two-dimensional motion.

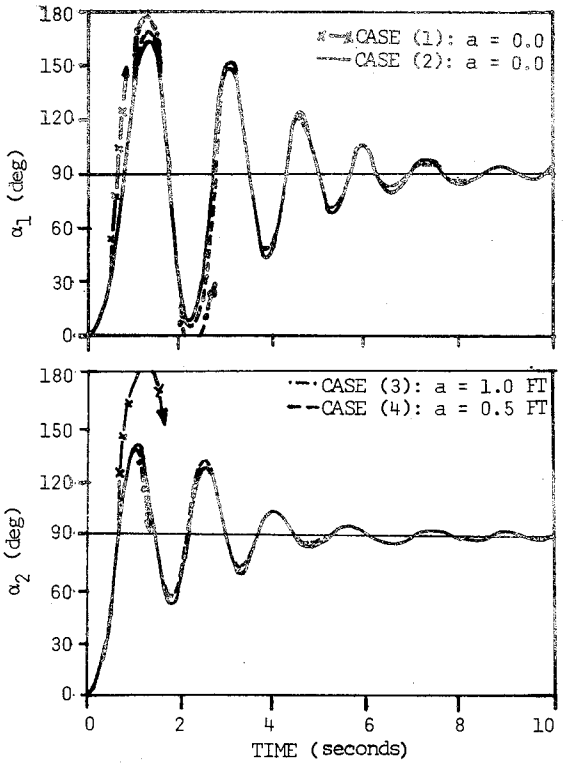

Fig. 3 Deployment dynamics of the system for three-dimensional motion.

However, it can be seen from consideration of the signs of each of the coefficients in Eq. (14) that $p_1>0$ and $p_3>0$. Since both g and n are positive, therefore, for stability, $\rho>0$, implying the necessity of (positive) hinge damping.

Case b: I_3 maximum moment of inertia ($n>0$) with offset of hinge points ($h\neq 0$): the details of the stability analysis are given in Ref. 2. The necessary condition from the rule of signs is obtained as

$$|a| \leq \sqrt{(I_3-I)/2m} \tag{17}$$

This inequality shows that the magnitude of hinge offset from the (1,2) hub plane is limited by the differences in the hub moments of inertia and the size of the end masses. The Routh-Hurwitz stability conditions obtained are of the same form as for the case of $h=0$.

Simulation Results

The nonlinear equations of motion, Eqs. (1-4), describing the deployment of the hinged system are used for numerical integration with the following system parameters[1] (Fig. 1):

$I_1=I_2=8.5$ slug-ft^2; $I_3=10.5$ slug-ft^2; $r_0=1$ ft;

$\ell=4$ ft; $a=0$; $m=0.125$ slug; $\Omega=4.82$ rad/sec.

A. Two-Dimensional Motion

The deployment dynamics of the system starting from the position where the hinged members are initially parallel to the spin axis ($\alpha=0$) is simulated in Fig. 2 without hinge damping (solid curve) and with hinge damping (dotted curve). The X on the time axis represents the maximum time simulated by Lang and Honeycutt.[1] It is seen that without hinge damping, the hinged members exhibit a flapping-type motion as momentum is exchanged between the hinge and spin motions. Figure 2 verifies the closed-form analytic solution obtained relating spin rate with hinge angle [Eq. (8)] for the undamped case. Also indicated are the maximum and minimum spin rate obtained during the flapping motion, as predicted by Eq. (8). With hinge damping the system can be fully deployed in about 10 sec.

B. Three-Dimensional Motion

The general three-dimensional motion analysis for large amplitude (α_1 and α_2 are physically free to vary between 0 and 180°) is considered in this section. The results are illustrated in Fig. 3 for different parameters. The rate damping torques about the '1' and '2' axes are assumed to be $-R_d\omega_1$, and $-R_d\omega_2$, respectively. From the simulation results, the observations are:

Case 1): for the values $a=0$, $c_\alpha=0$ and $R_d=0$, the hinge members would intersect the hub structure ($|\alpha|>180°$) as indicated.

Case 2): for the values $a=0$, $c_\alpha=0.1$ lb/ft/sec and $R_d=2$ lb-ft-sec, the hinge motion lies within the physical boundary as indicated, and the system can be fully deployed in about 10 sec. The angular rates about the transverse axes are nearly removed and the spin rate reaches a steady-state value of 4.1 rad/sec from an initial value of $\omega_3(0)=4.82$ rad/sec.[2]

Case 3): for the values: $a=1.0$ ft, $c_\alpha=0.1$ lb/ft/sec and $R_d=2$ lb-ft-sec, the hinge motion would interfere with the main satellite structure.

Case 4): since there are no criteria to determine the magnitude of offset of the hinge points for general nonlinear motion, a value of $a=0.5$ ft, which is less than 1.0 ft used in Case 3), is selected keeping the same values for c_α and R_d as in Case 3). The response of the system for these parameters is indicated. The behavior here is similar to that shown in Case 2).

Acknowledgments

Research supported by NASA Grant No. NSG-1181; special appreciation to C.W. Martz and W. Anderson, NASA-Langley, for helpful discussions.

References

[1]Lang, W. and Honeycutt, G.H., "Simulation of Deployment Dynamics of Spinning Spacecraft," NASA TN D4074, Aug. 1967.

[2]Bainum, P.M. and Sellappan, R., "The Dynamics of Spin Stabilized Spacecraft with Movable Appendages," Part II, Final

Report, NASA Grant NSG-1181, Howard University, Dept. of Mechanical Engineering, Washington, D.C., May 1976.

[3]Bainum, P.M., Fuechsel, P.G., and Mackison, D.L., "Motion and Stability of a Dual-Spin Satellite with Nutation Damping," *Journal of Spacecraft and Rockets*, Vol. 7, June 1970, pp. 690-696.

Minimization of Temperature Distortion in Thermocouple Cavities

Ching Jen Chen* and Peter Li†
The University of Iowa, Iowa City, Iowa

Introduction

A DIRECT measurement of transient surface temperature and heat flux is often difficult. For example, a surface involves two modes of heat transfer, say radiative and convective heat transfer. In this case, if the measuring probe has a different radiative property from that of the surface, erroneous measurements will result. Therefore, indirect estimation by inverting the temperature history inside the heat conducting solid as measured by a thermocouple is often used for prediction of the surface temperature and heat flux. Beck,[1] Herring and Parker,[2] Frank,[3] Imber and Khan,[4] Stolz,[5] and Chen and Thomsen[6] have developed inversion solutions for this purpose. Since all of these solutions assumed that the cavity drilled into the solid does not distort the true temperature distribution, it is, therefore, important that the temperature measurement by an interior probe be accurate and involve little distortion or error. From studies made by Chen and Li[7] and Beck,[8] it was found that with a proper combination of the thermocouple cavity diameter, cavity depth, and the thermocouple material, the magnitude of the distortion of the temperature field with respect to space or time can be minimized. In this Note we study the optimum combination of geometrical parameters and material properties to eliminate the temperature distortion.

Analysis

In the present study, we consider a disk depicted in Fig. 1, which has a thickness D and a cavity of diameter d drilled to a depth of ϵ distance from the heated surface. The heat flux Q is assumed to be constant and the upper surface of the disk is assumed to be insulated. A thermocouple of diameter d_t is welded onto the cavity base. The diameter of the disk is chosen to be $2D$ with the temperature distortion due to the thermocouple cavity assumed to be negligible at the edge. For this to be true Chen and Li[7] showed that the ratio of the cavity diameter to the disk diameter $d/2D$ should be smaller than 0.1. The portion of the cavity not filled by the thermocouple can be air or insulating material. The basic idea used to minimize or to eliminate the temperature distortion is based on a proper choice of the thermocouple size and the thermocouple material, which has a higher thermal conductivity than that of the disk, so as to conduct more heat away at the cavity base balancing the insulation effect of the insulator in the cavity.

Let X and Y be the respective coordinates along the heated disk surface and the axis of the cavity. The thermal conductivity is assumed to be constant. The governing equations for transient heat conduction in dimensionless form are

$$\frac{\partial\theta}{\partial\tau}=\frac{\alpha_i}{\alpha_1}\left(\frac{\partial^2\theta}{\partial x^2}+\frac{1}{x}\frac{\partial\theta}{\partial x}+\frac{\partial^2\theta}{\partial y^2}\right), \quad i=1,2,3 \tag{1}$$

where $\tau=\alpha_1 t/D^2$ is the dimensionless time, $x=X/D$ the dimensionless radial coordinate, and $y=Y/D$ the dimensionless distance normal to the heated surface. The α_i are the thermal diffusivities with subscripts 1, 2, and 3 denoting the disk, the insulating material, and the thermocouple. The dimensionless temperature θ is defined as $T\kappa_1/QD$ where T is the temperature above the initial uniform temperature and κ_1 is the thermal conductivity of the disk.

The initial temperature of the disk is

$$\theta(x,y,0)=0 \tag{2}$$

The boundary conditions (Fig. 1) are:

$$y=0,\ \left.\frac{\partial\theta}{\partial y}\right|_{y=0}=-1 \qquad y=1,\ \left.\frac{\partial\theta}{\partial y}\right|_{y=0}=0 \tag{3}$$

$$x=1,\ \left.\frac{\partial\theta}{\partial x}\right|_{x=1}=0 \qquad x=0,\ \left.\frac{\partial\theta}{\partial x}\right|_{x=0}=0 \tag{4}$$

There are five parameters that can be varied for the present analysis. They are: 1) the dimensionless distance from the base of the cavity to the heated surface ϵ/D, 2) the size of the cavity $d/2D$, 3) the ratio of the thermocouple diameter to that of the cavity d_t/d, 4) thermal conductivity ratios κ_2/κ_1 and κ_3/κ_1 which come from the continuity of heat flux at interfaces, and 5) the ratio of the product of density and specific heat ρ_3c_3/ρ_1c_1.

Because of the complexity of the geometry and the multiplicity of materials, the finite element technique as discussed by Wilson and Nikel[10] is adapted. The present problem is subdivided into finite elements as required by the method. The cross section is subdivided into 121 finite elements with 12 dividing lines on both coordinates. Each element is defined by four nodal points where nodal points are denoted by intersections of the dividing lines. The solution at each node with respect to time is then obtained.

For numerical calculations three typical values of the distance from the heated surface to the base of the cavity ϵ/D are chosen. They are 0.02, 0.06, and 0.1. The cavity diameter is fixed at one tenth of the disk diameter. The thermocouple to

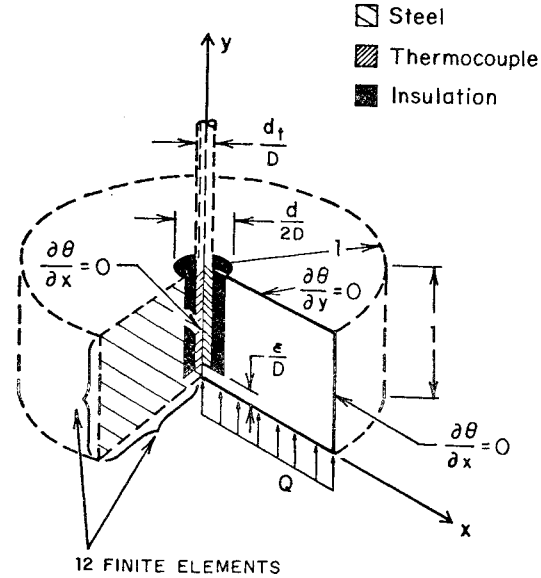

Fig. 1 Geometric representation of problem.

Received Oct. 20, 1976; revision received Feb. 28, 1977.

Index categories: Heat Conduction; Thermal Surface Properties; Rocket Engine Testing.

*Associate Professor, Dept. of Energy Engineering. Member AIAA.

†Research Assistant, Dept. of Energy Engineering.